Dual-ended readout of bismuth germanate to improve timing resolution in time-of-flight PET

Sun Il Kwon[1], **Emilie Roncali**[1], **Alberto Gola**[2], **Giovanni Paternoster**[2], **Claudio Piemonte**[2], **Simon R. Cherry**[1]

[1]Department of Biomedical Engineering, University of California, Davis, Davis, CA 95616, USA

[2]Fondazione Bruno Kessler, Trento, Italy

Abstract

The scintillator bismuth germanate (BGO) has attractive properties for positron emission tomography (PET) systems such as high stopping power, high photo-fraction, and relatively low cost. However, its moderate scintillation light yield and slow rise and decay time compared to lutetium (yttrium) oxyorthosilicate (L(Y)SO) results in a degradation of coincidence timing resolution when scintillation photons are used for timing. Recently, it has been reported that the coincidence timing resolution of BGO can be improved by detecting Cerenkov photons, while scintillation photons still provide energy information. However, the measured coincidence timing spectrum showed much longer tails compared to the single Gaussian distribution. Because of this, TOF PET detectors based on BGO will perform worse than the full width at half maximum (FWHM) of the distribution, which is the most common metric for timing resolution, would suggest. From simulation studies, during the first few picoseconds, BGO generates ~16 Cerenkov photons per photoelectric interaction, following a 511 keV gamma ray interaction, while the probability of producing a scintillation photon during the first few picoseconds is very small. Therefore, when we configure a BGO crystal with dual-ended readout, the first arriving photons among the two opposing SiPMs are most likely Cerenkov photons, and by selecting the appropriate SiPM, an improvement in coincidence timing resolution can be achieved. In this study, both ends of a $3 \times 3 \times 20$ mm^3 BGO crystal were coupled to NUV-HD SiPMs. Trigger time differences from the dual-ended readout of BGO were widely distributed due to detecting a mixture of prompt Cerenkov and scintillation photons on both SiPMs. When using trigger times from only a single SiPM, the estimated coincidence timing resolution between two identical BGO detectors was 463 ps FWHM and 1463 ps FWTM. In contrast, when using trigger times from both SiPMs, the estimated coincidence timing resolution was 399 ps FWHM and 936 ps FWTM with no loss of events. Based on a recent report, high-bandwidth amplifiers were implemented and shown to further improve the estimated coincidence timing resolution to 331 ps FWHM and 923 ps FWTM. In summary, the coincidence timing resolution of BGO, most notably the FWTM, was significantly improved using time information from the dual-ended readout.

sunkwon@ucdavis.edu.

1. Introduction

Bismuth germanate (BGO) still has more attractive properties for the use in positron emission tomography (PET) scanners compared to current popular scintillators such as lutetium oxyorthosilicate (LSO) and lutetium-yttrium oxyorthosilicate (LYSO). It has a high atomic number, density, and photo-fraction for 511 keV gamma rays (Humm *et al.* 2003, Moses 2007). It also has no background activity and can be produced with relatively lower cost than lutetium-based scintillators. BGO is therefore an attractive candidate for next generation long axial field-of-view PET scanners which require large volumes of scintillator material (Cherry *et al.* 2018). However, a major drawback of BGO was poor timing performance (Moses 2007, Szczesniak *et al.* 2013) originating from the moderate light yield and slow rise and decay times of scintillation photon production (Moszyński *et al.* 1981). Therefore, BGO had not been considered for the use in current PET scanners which incorporate time-of-flight (TOF) information to improve image quality (Surti 2015).

When a 511 keV annihilation gamma ray interacts with a BGO scintillator, a small number of Cerenkov photons are promptly produced within a few picoseconds by an energetic electron (Williams *et al.* 2001). Since the production of Cerenkov photons by the conversion of a 511 keV gamma ray is quasi-instantaneous, the Cerenkov photons can potentially improve timing performance (Lecoq *et al.* 2010), especially in BGO that has a high refractive index (2.15 at 480 nm) and excellent optical transparency down to 320 nm (Williams *et al.* 1996, Rihua *et al.* 2008). Development of SiPM technologies enables detection of the faint Cerenkov radiation, resulting in dramatic improvement in coincidence timing resolution of BGO (Kwon *et al.* 2016, Brunner and Schaart 2017). Consequently, PET detectors with good TOF capability can likely be constructed using BGO scintillator. In a TOF PET detector based on BGO, the timing and energy information of each gamma event can be obtained using Cerenkov and scintillation photons, respectively.

Figure 1 shows one of our recent coincidence timing spectra measured from a coincidence setup composed of two identical BGO detectors and a ^{22}Na point source. Each BGO detector consisted of a $3 \times 3 \times 20$ mm^3 BGO scintillator and an NUV-HD SiPM (FBK, Trento, Italy) (Gola *et al.* 2019), which attached to the opposite surface from the gamma entrance surface in the BGO pixel. Each BGO pixel was polished and wrapped with polytetrafluoroethylene (PTFE) tape. As shown in Figure 1 and other previous results (Kwon *et al.* 2016, Brunner and Schaart 2017), coincidence timing resolution represented by the full width at half maximum (FWHM) of BGO was within an appropriate range for TOF PET detectors. However, the coincidence timing spectrum is not well fit by a single Gaussian and had a much larger full width at tenth maximum (FWTM) compared to other fast scintillators, such as LSO, LYSO, LGSO, and LaBr3:Ce (Schaart *et al.* 2010, Ito *et al.* 2013, Schmall *et al.* 2014, Cates and Levin 2016). This is caused by detecting a mixture of prompt Cerenkov and scintillation photons at each photosensor. Because of these long tails, TOF PET detectors based on BGO will not be able to fully benefit from the much improved FWHM.

From our previous simulation study (Kwon and Cherry 2017) and calculations using Frank-Tamm formula, during the first few picoseconds, BGO generates ~16 Cerenkov photons per photoelectric interaction over a spectral range of 320–800 nm, when a 511 keV gamma ray

interacts with BGO. In this case, the earliest Cerenkov photons are preferentially emitted in the forward direction (incident direction of a 511 keV gamma ray). Later emitted Cerenkov photons gradually lose this directionality. Thus, we ultimately observe Cerenkov photons emitted in all directions. However, the number of emitted photons per solid angle is not uniform because of the directionality of the earliest emitted Cerenkov photons. Therefore, Cerenkov production in BGO can be considered as quasi-isotropic emission. Meanwhile, statistically, it takes over 400 ps to emit the same number of scintillation photons in BGO when the fast (60 ns) and slow (300 ns) decay components (Moszyński *et al.* 1981) are considered, assuming an infinitely fast rise time. Based on these properties, in BGO, we consider that Cerenkov photons are emitted quasi-isotropically and simultaneously and earlier than scintillation photons, while scintillation photons are emitted isotropically but not simultaneously. Therefore, when we configure BGO with a dual-ended readout, the first detected photons on one of the two opposing photosensors are more likely prompt Cerenkov photons due to the slow and sparse generation of scintillation photons. Consequently, we hypothesize that dual-ended readout of BGO, with appropriate choice of which SiPM to trigger from, can further improve the coincidence timing resolution, especially the FWTM. In this study, we show improvement in the timing performance of BGO by using timing information from both photodetectors at both ends of BGO.

2. Materials and Methods

2.1. Experimental setup

Figure 2 shows the experimental setup. Coincidence events from a ^{22}Na point source were acquired using a BGO detector and a reference detector. In the BGO detector, one polished 3 × 3 × 20 mm^3 BGO pixel (SICCAS, China) was prepared and wrapped in three layers of PTFE tape. The BGO pixel was read out from both ends by two NUV-HD SiPMs (FBK, Trento, Italy) coupled to the BGO pixel through optical grease. The NUV-HD SiPM has low noise and very high photon detection efficiency (PDE) across a broad wavelength range, especially in the UV/blue region (Kwon *et al.* 2016). PTFE was used as the reflector because it has better reflectivity than other common reflectors in the critical range of 300–400 nm (Janecek 2012). In the reference detector, a polished 3 × 3 × 5 mm^3 LYSO crystal wrapped with PTFE tape was coupled to an RGB-HD SiPM (FBK, Trento, Italy). Silicone optical grease (BC-630, Saint-Gobain Crystals) was used for optical coupling between pixels and SiPMs. It has a refractive index of 1.465 and a very flat transmittance of ~95% for wavelengths down to 280 nm based on data provided by Saint-Gobain Crystals. Each SiPM was connected to a custom amplifier, which provided an energy output and a timing output filtered with a pole-zero cancellation circuit (Gola *et al.* 2013). The BGO detector and the reference detector faced each other with the top SiPM facing toward the reference detector. Output signals were digitized with a high-performance oscilloscope (DPO71254C, Tektronix) at a sampling rate of 50 GS/s (20 ps time bin) and a bandwidth of 3 GHz in order to acquire precise time information from each SiPM. Since the oscilloscope has only four channels and one external trigger channel, as shown in Figure 2, two timing signals from the BGO detector and one timing signal from the reference detector were respectively connected to channels 1, 4, and 2 of the oscilloscope. One energy signal from the bottom SiPM of the BGO detector was connected to channel 3 of the oscilloscope in order to estimate the

deposited energy of each gamma event. Coincidence events were determined by a coincidence logic unit using the energy signal from the reference detector and the energy signal from the bottom SiPM of the BGO detector. Dedicated 3D-printed holders were used to ensure alignment between detectors. Temperature was maintained at 20 °C.

Digitized energy signals from the BGO detector and timing signals from the reference detector were integrated to calculate the energy of each coincidence event. The resulting energy values were histogrammed to form the energy spectrum. The 511-keV photopeak region was fitted with a single Gaussian. Coincidence events within the FWTM around the 511-keV photopeak were used for timing analysis. The trigger time of each timing signal was determined by leading edge thresholding after linear interpolation. Trigger times for the top (t_T) and bottom (t_B) SiPMs of the BGO detector used thresholds which were able to trigger on a single photon. Therefore, the trigger time from the top or bottom SiPM (t_T or t_B) represents the time of the first detected photon on each SiPM. Trigger times of the reference detector (t_{ref}) were also calculated to determine coincidence timing resolution. To estimate the contribution of the BGO detector to the coincidence timing resolution, the single timing resolution of the reference detector was measured using three different detectors, one of which was the reference detector. Coincidence timing resolutions for all three possible pairs were first obtained. The single timing resolution of the reference detector was then derived as 154 ps FWHM and 281 ps FWTM from a system of linear equations (Ito *et al.* 2013).

2.2. Monte Carlo simulation

To aid in interpreting the experimental data, Monte Carlo simulations were also conducted using the LUT Davis model implemented in GATE V8.0 (Stockhoff *et al.* 2017), which can study the transport and detection of optical photons. In the simulation study, two identical BGO detectors were configured instead of the real experimental setup. Simulation parameters were set to generate both Cerenkov and scintillation photons. BGO was modeled with 10% fast (60 ns) decay component, 90% slow (300 ns) decay component (Moszyński *et al.* 1981), and no rise time. The scintillation yield of BGO was set to 8000 ph/MeV, and the measured emission spectrum of BGO was obtained from the previous literature (Kwon *et al.* 2016). A variable refractive index based on wavelength was applied (Williams *et al.* 1996). For each coincidence event, all photons arriving at each end of BGO were recorded with information including generation type (Cerenkov or scintillation) and arrival time. Since this simulation study mainly focused on how the contributions of Cerenkov and scintillation photons change the shape of the timing spectrum, we only considered PDE and time variations in order to approximate the SiPM and amplifiers response and implemented this in MATLAB. The measured PDE curve for an NUV-HD SiPM (Kwon *et al.* 2016) was used. For the time variations, we used a Gaussian function in order to add time variations into photon detection times. A sigma value of the Gaussian function was estimated based on single photon time resolution (Nemallapudi *et al.* 2016), and we slightly increased the value to also consider electronic jitter. A sigma value of 110 ps was used. Optical grease coupling was not modeled. The trigger time of each SiPM was defined as the detection time of the first photon.

3. Results and discussion

3.1. Trigger time difference within the BGO detector

After recording coincidence events, the trigger time difference (t_B - t_T) between the bottom and top SiPMs of the BGO detector was calculated. The distribution of the trigger time differences is shown in Figure 3(a) and was widely distributed between −2000 ps and 2000 ps because of the slow and sparse generation of scintillation photons in BGO. The peak of the curve was shifted to the right of 0 ns. The primary reason is that more gamma rays interacted near the top SiPM, so the photon-travel times and subsequent detection times at the bottom SiPM are slightly longer than those for the top SiPM. As shown in Figure 3(b), the distribution of the trigger time difference from simulations also was widely distributed between −2000 ps and 2000 ps, similar to the distribution from the experimental results (black line in each figure). In the simulation results, the distribution can be divided into four different cases depending on the type of the photon which triggered each SiPM; i) both SiPMs were triggered by Cerenkov photons [blue line in Figure 3(b)], ii) and iii) either the bottom or top SiPM was triggered by Cerenkov photons (green and orange, respectively), and iv) neither SiPM was triggered by Cerenkov photons (red). In case i), the trigger time differences form a much narrower distribution between −500 ps and 600 ps (99.5% of events are within this region) because promptly emitted Cerenkov photons triggered both SiPMs. In contrast, long tails appeared in the distribution when scintillation photons triggered one or both SiPMs. For the PDE of these SiPMs, selected energy window, and trigger thresholds, the probabilities of each case are: 41% for case i), 26% for case ii), 19% for case iii), and 14% for case iv). Consequently, we can confirm that triggering on the scintillation photons caused the wide distribution of the trigger time difference between the bottom and top SiPMs.

3.2. Coincidence timing resolution

Trigger times from either the top or bottom SiPM can be used to determine coincidence timing resolution between the BGO detector and the reference detector. When the bottom SiPM of the BGO detector is used to calculate coincidence time differences with the reference detector (t_B - t_{ref}), we can filter out coincidence events where the optical photons generated in BGO trigger the bottom SiPM a certain time (K_1) later than the top SiPM. The coincidence events filtered out by this rule have a high probability that the optical photons triggering the bottom SiPM are not the earliest produced photons. After the filtering, coincidence time differences (t_B - t_{ref}) of the remaining coincidence events, which meet the condition ($t_B - t_T \leq K_1$), were histogrammed to form the coincidence timing spectrum between the two detectors. The FWHM and FWTM were extracted from each timing spectrum by fitting the experimental data with four Gaussians. Figures 4(a)-(c) show coincidence timing spectra with different Ki values of 1500 ps, 600 ps, and 0 ps, respectively. When the K_1 value decreases from 1500 ps to 600 ps, the FWHM of 362±4 ps was not changed while the FWTM decreased from 1072±22 ps to 892±12 ps. When we further reduce K_1 to 0 ps, it was observed that not only FWTM but also FWHM decreased to values of 666±14 ps and 302±3 ps, respectively. Figure 5(a) shows how the FWHM and FWTM changes as K_1 is varied from 0 ps to 2000 ps. As shown in Figure 5(a), the FWTM starts improving earlier than the FWHM with decreasing K_1. The interpretation of this result

is that the t_B - t_T filter with K_1 first excludes coincidence events which were triggered by scintillation photons on the bottom SiPM of the BGO detector. The FWHM also improved when K_1 was lower than ~600 ps. In this time region, since gamma interaction events where Cerenkov photons trigger both top and bottom SiPMs are most probable as shown in Figure 3(b), we can consider that the time difference (t_B - t_T) is roughly proportional to the depth of a gamma interaction. Therefore, both FWHM and FWTM can improve by excluding events that occur far from the bottom SiPM. However, when the K_1 value reduces from i500 ps to 0 ps, the number of remaining coincidence events decreased by more than half (from 136k to 64k) as shown in Figures 6(a) and (c).

Similar patterns also emerged when the top SiPM was used to determine coincidence timing resolution with the reference detector (t_T - t_{ref}). In this case, we can filter out coincidence events where the optical photons generated in BGO trigger the top SiPM a certain time ($-K_2$) later than the bottom SiPM. The FWHM and FWTM as a function of K_2 were calculated using the coincidence events that meet the condition (t_B - t_T $\geq K_2$). As shown in Figure 5(b), the FWTM starts improving much earlier than FWHM as K_2 is increased towards 0 ps. Coincidence timing resolution was 475±7 ps FWHM and 1205±24 ps FWTM at K_2= −1500 ps, and 339±4 ps FWHM and 755±16 ps FWTM at K_2= 0 ps. Coincidence timing resolution using the bottom SiPM was better than that using the top SiPM. The main reasons are i) the earliest Cerenkov photons are preferentially emitted in the forward direction, resulting in more Cerenkov photons arriving at the bottom SiPM (Brunner *et al.* 2014, Somlai-Schweiger and Ziegler 2015, Kwon and Cherry 2017) and ii) propagation velocities of scintillation light versus 511 keV photons are different (Derenzo *et al.* 2015).

As shown in Figures 6(a) and 6(b), the simulation study recapitulated the patterns of the experimental results shown in Figures 5(a) and 5(b). Similar to experimental results, the FWTM started improving with K_1 and K_2 earlier than the FWHM. Figure 6(c) shows the number of events which were triggered by Cerenkov (blue line) or scintillation (green line) photons on the bottom SiPM as a function of time filtering threshold K_1. The total number of events (black line) is also shown in Figure 6(c). Similarly, Figure 6(d) shows the case when the top SiPM was used for determining coincidence timing resolution with threshold K_2. As shown in Figures 6(c) and (d), as the absolute values of K_1 and K_2 decrease, time filtering (t_B - t_T) first eliminates events triggered by scintillation photons and then later starts filtering out events triggered by Cerenkov photons. These findings closely correlate with the coincidence timing resolution represented by the FWHM Based on the experiments and simulations, the large FWTM in the coincidence timing spectrum between the two detectors can be much reduced by time filtering between top and bottom SiPMs. The FWHM also improved using the time filtering.

3.3. Adaptive time difference calculation

We demonstrated that the FWHM and FWTM of the coincidence timing spectrum were improved by using (t_B - t_T) time filtering. However, in both cases, events are being eliminated to improve coincidence timing resolution. This causes degradation of detector sensitivity which would not be acceptable. Therefore, to improve coincidence timing resolution with no loss of events, we propose an adaptive time difference calculation by

combining these two cases. For the proposed method, first, we define a new variable k by setting K_1 equal to K_1. Then if optical photons trigger the bottom SiPM a certain time (k) later than the top SiPM, the proposed method uses the trigger time (t_B) from the top SiPM for determining coincidence timing resolution, otherwise, it uses the trigger time (t_T) from the bottom SiPM. This rule is expressed in Equation 1.

$$\Delta t_{\text{coincidence}} = \begin{cases} t_B - t_{\text{ref}}, t_B - t_T \leq k \\ t_T - t_{\text{ref}}, t_B - t_T > k \end{cases} \tag{1}$$

Using the proposed method, the coincidence timing resolution using the same data in the previous sections were calculated as a function of k (Figure 7). Coincidence timing resolution showed that the best results are obtained when the value of k was near zero. This means that the coincidence timing resolution can be improved by simply using the earliest trigger time between the top and bottom SiPMs for each event. Regardless of the value k, the number of coincidence events used to determine coincidence timing resolution remains unchanged.

For comparison, we analyzed the same data using a traditional method and the proposed method, respectively. The traditional method modeled a single-ended readout BGO detector and used only trigger times from the bottom SiPM to calculate coincidence timing resolution. Since the top surface of the BGO crystal was covered by an SiPM, instead of a reflector, we refer to this as a quasi-single-ended BGO detector. Figure 8(a) shows a coincidence timing spectrum between the reference detector and the quasi-single-ended BGO detector. The coincidence timing resolution was 362±4 ps FWHM and 1072±21 ps FWTM. The single timing resolution of the quasi-single-ended BGO detector was calculated by quadratic subtraction (Schmall *et al.* 2014), and then multiplied by $\sqrt{2}$ to estimate coincidence timing resolution between two identical quasi-single-ended BGO detectors. The estimated coincidence timing resolution was 463 ps FWHM and 1463 ps FWTM. These values well agree with our previous measurement shown in Figure 1. In contrast, Figure 8(b) shows coincidence timing spectrum generated by using the proposed method when k is equal to 0. The coincidence timing resolution was 322±3 ps FWHM and 719±11 ps FWTM. With the same calculation, when we configure two identical dual-ended readout BGO detectors with the proposed method, the estimated coincidence timing resolution was 399 ps FWHM and 936 ps FWTM. By using the proposed method, FWHM and FWTM were significantly improved by 64 ps and 528 ps, respectively, with no loss of events.

Dual-ended readout of scintillation material is a popular configuration for depth-of-interaction (DOI) PET detectors that provide the depth of gamma interaction for each event to improve spatial resolution at off-center locations (Chaudhari *et al.* 2008, Ito *et al.* 2011, Yang *et al.* 2016). Therefore, we can also expect DOI capability for this dual-ended readout BGO detector. To briefly estimate DOI capability of the detector, we performed additional experiments by connecting the energy signal of the top SiPM to channel 4 of the oscilloscope instead of the timing signal of the top SiPM. Side-on measurements were performed using electronic collimation (Schmall *et al.* 2014) with a ^{22}Na point source. The estimated width of the collimating beam at the crystal was 1.5 mm. Coincidence events at

three different depth positions (2 mm, 10 mm, and 18 mm from the bottom SiPM face) were acquired. The DOI ratio was defined as the ratio of energy measured at the top SiPM over the summed energy from the top and bottom SiPMs. The average DOI resolutions (Chaudhari *et al.* 2008) of the BGO detector at 2 mm, 10 mm, and 18 mm irradiation depths were 13.5±0.4 mm, 11.0±0.3 mm, and 11.7±0.4 mm, respectively, without beam width correction. Since this study only focused on timing, we expect that DOI performance can be improved by further optimization.

Meanwhile, there also are some studies that proposed dual-ended readout to improve coincidence timing resolution, especially for LYSO or other fast scintillators (Derenzo *et al.* 2015, Kang *et al.* 2015, Seifert and Schaart 2015, Derenzo 2017). In those studies, trigger times from the dual-ended readout were mainly used to correct depth-dependent variations, and coincidence timing resolution improved using depth-corrected trigger times or an average of the top and bottom trigger times. For comparison, we performed an additional experiment by replacing the BGO crystal with a polished $3 \times 3 \times 20$ mm^3 LYSO crystal in our experimental setup. However, our proposed method did not improve coincidence timing resolution of LYSO. The coincidence timing resolution calculated using our proposed method (208±2 ps FWHM at *k=0*) was slightly worse than that obtained by using trigger times from only the bottom SiPM (198±1 ps FWHM), and much worse than that calculated by using the average method (180±1 ps FWHM). The reason why the proposed method in this study was more effective in BGO than in a fast and bright scintillator such as LYSO is that BGO emits scintillation photons much more slowly than Cerenkov photons, and also that BGO produces more Cerenkov photons than LYSO. So, in BGO, the trigger time difference of the dual-ended readout is strongly influenced not only by interaction depth but also by the type (Cerenkov or scintillation) of the emitted photons. For this reason, averaging the two trigger times from the dual-ended readout of BGO did not improve coincidence timing resolution. The estimated coincidence timing resolution results for different triggers from the BGO detector are summarized in Table 1.

Recently, it was reported that high-bandwidth amplifiers can improve the measured single photon time resolution (SPTR) (Cates *et al.* 2018, Gundacker *et al.* 2019), resulting in an improved coincidence timing resolution between two PET detectors. Based on the study by (Gundacker *et al.* 2019), a high-bandwidth amplifier was implemented and employed in this study. The same transformer (MABA-007159, Macom) and RF-amplifiers (BGA616, Infineon) were used for high-bandwidth amplification, and its output signal was used as a timing signal. A two-stage operational amplifier circuit was also implemented in order to acquire energy information for each event. Two amplifier boards were prepared and replaced the existing amplifiers on the BGO detector, while the reference detector remained unchanged. Since the high-bandwidth board also has timing and energy outputs, the experimental setup was the same as shown in Figure 2. Figure 9 shows the coincidence timing spectrum acquired using the high-bandwidth amplifiers and the proposed method with *k*=0. The measured coincidence timing resolution was 280±1 ps FWHM and 711±6 ps FWTM. For two identical dual-ended readout BGO detectors with the proposed method, the estimated coincidence timing resolution is 331 ps FWHM and 923 ps FWTM. Thus, a further improvement was achieved using the proposed method combined with high-bandwidth amplifiers, and these results improve on previously reported results at room

temperature, especially in terms of the FWTM (Kwon *et al.* 2016, Brunner and Schaart 2017).

4. Conclusions

BGO has been an attractive scintillator for PET scanners and now can be considered as a relevant scintillator for TOF PET scanners by detecting prompt Cerenkov photons. With single ended-readout, the large FWTM observed in the coincidence timing spectrum will degrade performance even though the FWHM is fairly narrow. In this study, to resolve this issue, the dual ended-readout method was adopted to increase the probability of detecting and identifying prompt Cerenkov photons, resulting in a very significant improvement in coincidence timing resolution. Experimental and simulation studies were conducted to understand trigger time differences for dual-ended readout of BGO. Based on the results, we proposed an adaptive time difference calculation method which improves both FWHM and FWTM of the coincidence timing resolution. Using the proposed method, the large FWTM in the coincidence timing spectrum was dramatically reduced with no loss of events. In addition to the improvement in coincidence timing resolution, the dual-ended readout of BGO can also provide depth information. Since the proposed method simply uses the time difference of the dual-ended readout, it is expected that the method can be easily implemented for detector level applications. We will do further studies to improve DOI performance and to reduce the number of signals for PET block detectors.

Acknowledgments

References

Brunner SE, Gruber L, Marton J, Suzuki K and Hirtl A 2014 Studies on the Cherenkov Effect for Improved Time Resolution of TOF-PET Ieee TNucl Sci 61 443–7

Brunner SE and Schaart DR 2017 BGO as a hybrid scintillator/Cherenkov radiator for cost-effective time-of-flight PET Phys. Med. Biol 62 4421–39 [PubMed: 28358722]

Cates JW, Gundacker S, Auffray E, Lecoq P and Levin CS 2018 Improved single photon time resolution for analog SiPMs with front end readout that reduces influence of electronic noise Physics in medicine and biology 63 185022

Cates JW and Levin CS 2016 Advances in coincidence time resolution for PET Physics in medicine and biology 61 2255–64 [PubMed: 26914187]

Chaudhari AJ, Yang Y, Farrell R, Dokhale PA, Shah KS, Cherry SR and Badawi RD 2008 PSPMT/APD Hybrid DOI Detectors for the PET Component of a Dedicated Breast PET/CT System; A Feasibility Study IEEE Trans. Nucl. Sci 55 853–61

Cherry SR, Jones T, Karp JS, Qi J, Moses WW and Badawi RD 2018 Total-Body PET: Maximizing Sensitivity to Create New Opportunities for Clinical Research and Patient Care J. Nucl. Med 59 3–12 [PubMed: 28935835]

Derenzo SE 2017 Monte Carlo simulations of time-of-flight PET with double-ended readout: calibration, coincidence resolving times and statistical lower bounds Phys. Med. Biol 62 3828–58 [PubMed: 28327464]

Derenzo SE, Choong WS and Moses WW 2015 Monte Carlo calculations of PET coincidence timing: single and double-ended readout Phys. Med. Biol 60 7309–38 [PubMed: 26350162]

Gola A, Acerbi F, Capasso M, Marcante M, Mazzi A, Paternoster G, Piemonte C, Regazzoni V and Zorzi N 2019 NUV-Sensitive Silicon Photomultiplier Technologies Developed at Fondazione Bruno Kessler Sensors (Basel) 19

Gola A, Piemonte C and Tarolli A 2013 Analog Circuit for Timing Measurements With Large Area SiPMs Coupled to LYSO Crystals IEEE Trans. Nucl. Sci 60 1296–302

Gundacker S, Martinez Turtos R, Auffray E, Paganoni M and Lecoq P 2019 High-frequency SiPM readout advances measured coincidence time resolution limits in TOF-PET Physics in medicine and biology

Humm JL, Rosenfeld A and Del Guerra A 2003 From PET detectors to PET scanners Eur J Nucl Med Mol Imaging 30 1574–97 [PubMed: 14579100]

Ito M, Hong S and Lee JS 2011 Positron emission tomography (PET) detectors with depth-of-interaction (DOI) capability Biomed. Eng. Lett 1 70–81

Ito M, Jin Pyo L and Jae Sung L 2013 Timing Performance Study of New Fast PMTs With LYSO for Time-of-Flight PET IEEE Trans. Nucl. Sci 60 30–7

Janecek M 2012 Reflectivity Spectra for Commonly Used Reflectors Ieee T Nucl Sci 59 490–7

Kang HG, Ko GB, Rhee JT, Kim KM, Lee JS and Hong SJ 2015 A Dual-Ended Readout Detector Using a Meantime Method for SiPM TOF-DOI PET IEEE Trans. Nucl. Sci 62 1935–43

Kwon SI and Cherry SR 2017 Simulation Study of the Generation of Cerenkov Photons in Bismuth Germanate for PET 2017 IEEE NSS/MIC Atlanta, Georgia, USA

Kwon SI, Gola A, Ferri A, Piemonte C and Cherry SR 2016 Bismuth germanate coupled to near ultraviolet silicon photomultipliers for time-of-flight PET Phys. Med. Biol 61 L38–L47 [PubMed: 27589153]

Lecoq P, Auffray E, Brunner S, Hillemanns H, Jarron P, Knapitsch A, Meyer T and Powolny F 2010 Factors Influencing Time Resolution of Scintillators and Ways to Improve Them IEEE Trans. Nucl. Sci 57 2411–6

Moses WW 2007 Recent Advances and Future Advances in Time-of-Flight PET Nucl. Instrum. Methods Phys. Res. A 580 919–24 [PubMed: 18836513]

Moszyński M, Gresset C, Vacher J and Odru R 1981 Timing properties of BGO scintillator Nucl. Instrum. Methods Phys. Res. A 188 403–9

Nemallapudi MV, Gundacker S, Lecoq P and Auffray E 2016 Single photon time resolution of state of the art SiPMs J. Instrum 11 P10016-P

Rihua M, Liyuan Z and Ren-Yuan Z 2008 Emission Spectra of LSO and LYSO Crystals Excited by UV Light, X-Ray and gamma ray Nuclear Science, IEEE Transactions on 55 1759–66

Schaart DR, Seifert S, Vinke R, Dam H T v, Dendooven P, Löhner H and Beekman FJ 2010 LaBr 3 :Ce and SiPMs for time-of-flight PET: achieving 100 ps coincidence resolving time Physics in medicine and biology 55 N179

Schmall JP, Roncali E, Berg E, Viswanath V, Du J and Cherry SR 2014 Timing properties of phosphor-coated polished LSO crystals Phys. Med. Biol 59 N139

Seifert S and Schaart DR 2015 Improving the Time Resolution of TOF-PET Detectors by Double-Sided Readout IEEE Trans. Nucl. Sci 62 3–11

Somlai-Schweiger I and Ziegler SI 2015 CHERENCUBE: Concept definition and implementation challenges of a Cherenkov-based detector block for PET Medical physics 42 1825–35 [PubMed: 25832073]

Stockhoff M, Jan S, Dubois A, Cherry SR and Roncali E 2017 Advanced optical simulation of scintillation detectors in GATE V8.0: first implementation of a reflectance model based on measured data Phys. Med. Biol 62 L1–L8 [PubMed: 28452339]

Surti S 2015 Update on time-of-flight PET imaging J. Nucl. Med 56 98–105 [PubMed: 25525181]

Szczesniak T, Kapusta M, Moszyński M, Grodzicka M, Szawlowski M, Wolski D, Baszak J and Zhang N 2013 MPPC Arrays in PET Detectors With LSO and BGO Scintillators IEEE Trans. Nucl. Sci 60 1533–40

Williams PA, Rose AH, Lee KS, Conrad DC, Day GW and Hale PD 1996 Optical, thermo-optic, electro-optic, and photoelastic properties of bismuth germanate (Bi4Ge3O12) Appl Optics 35 3562–9

Williams RT, Ucer KB and LoPresti JL 2001 In the first instants … ultrafast views of radiation effects Radiat. Meas 33 497–502

Yang Y, Bec J, Zhou J, Zhang M, Judenhofer MS, Bai X, Di K, Wu Y, Rodriguez M, Dokhale P, Shah K, Farrell R, Qi J and Cherry SR 2016 A high resolution prototype small-animal PET scanner dedicated to mouse brain imaging J. Nucl. Med
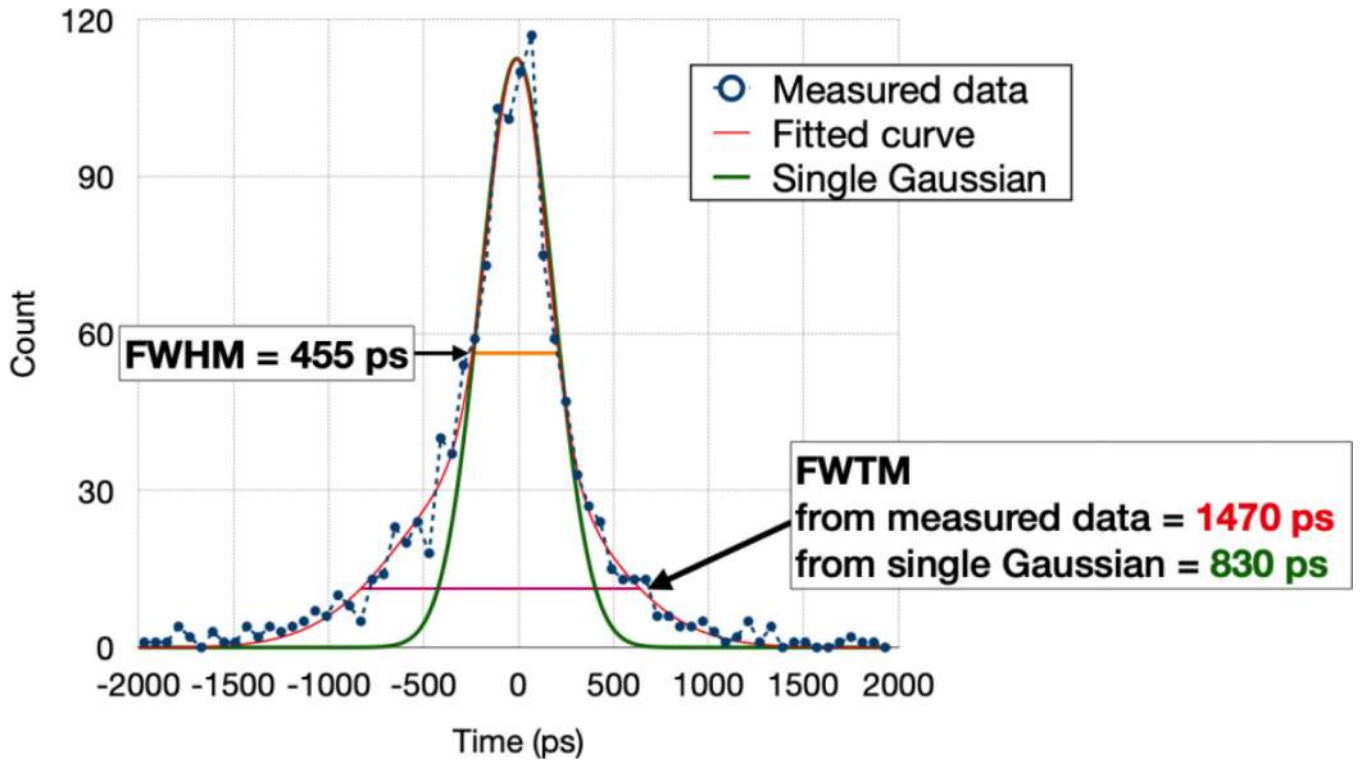
Figure 1.
Measured coincidence timing spectrum between two single-ended BGO detectors and single Gaussian fit (green). For the observed FWHM (455 ps), BGO has much larger FWTM (1470 ps) than that predicted by a single Gaussian fit (830 ps)
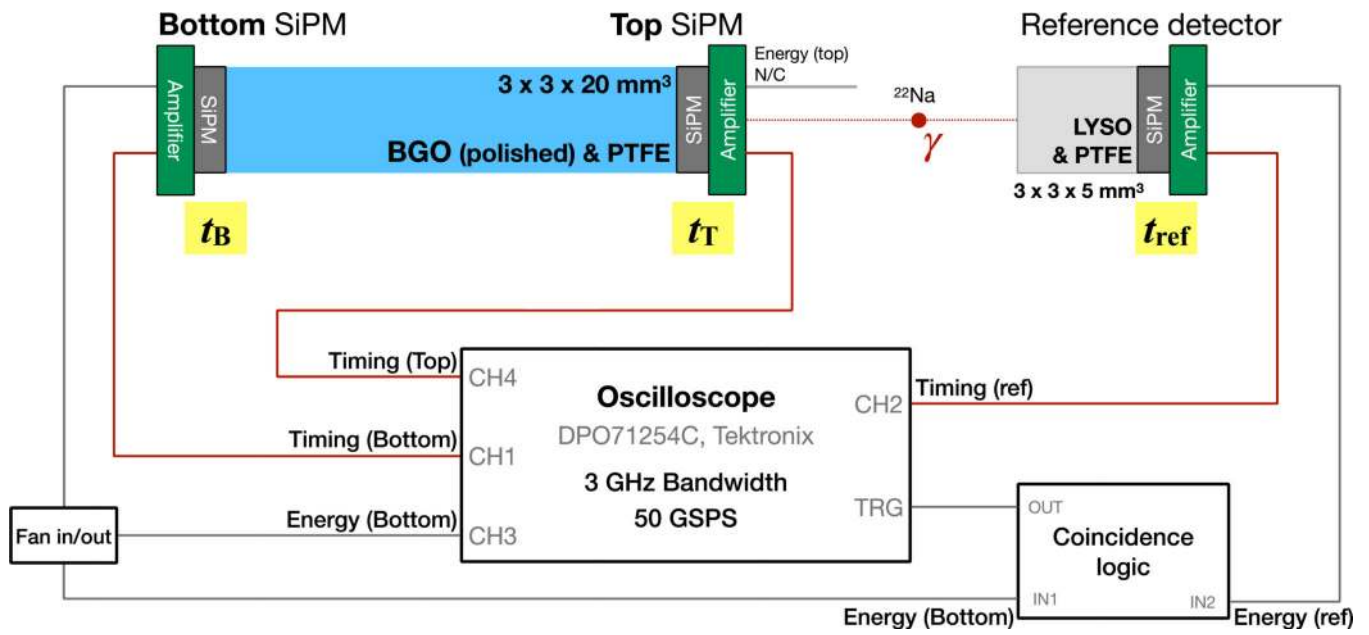
Figure 2.
Experimental setup for dual-ended readout of BGO and a reference detector.
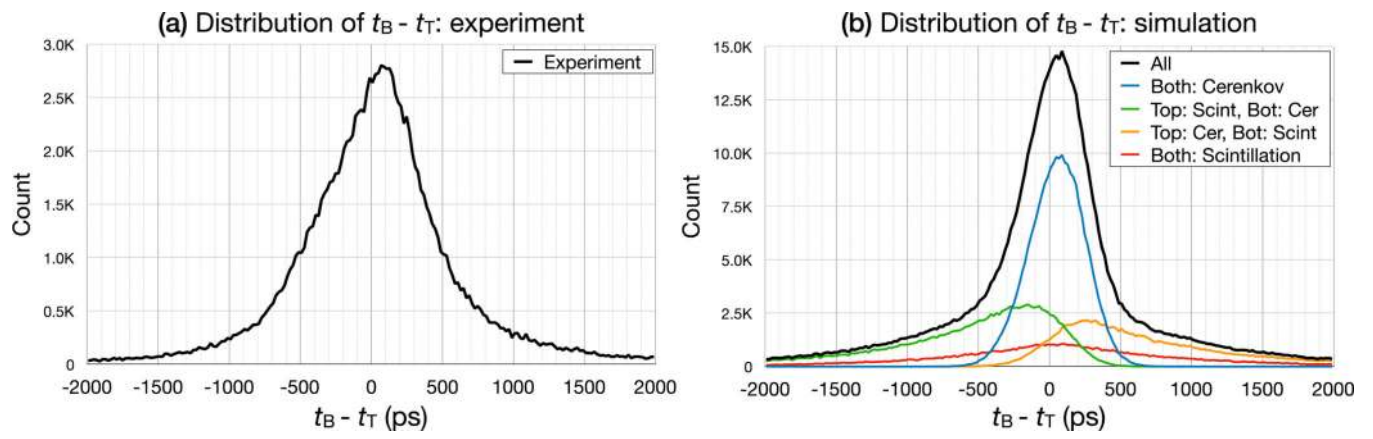
Figure 3.

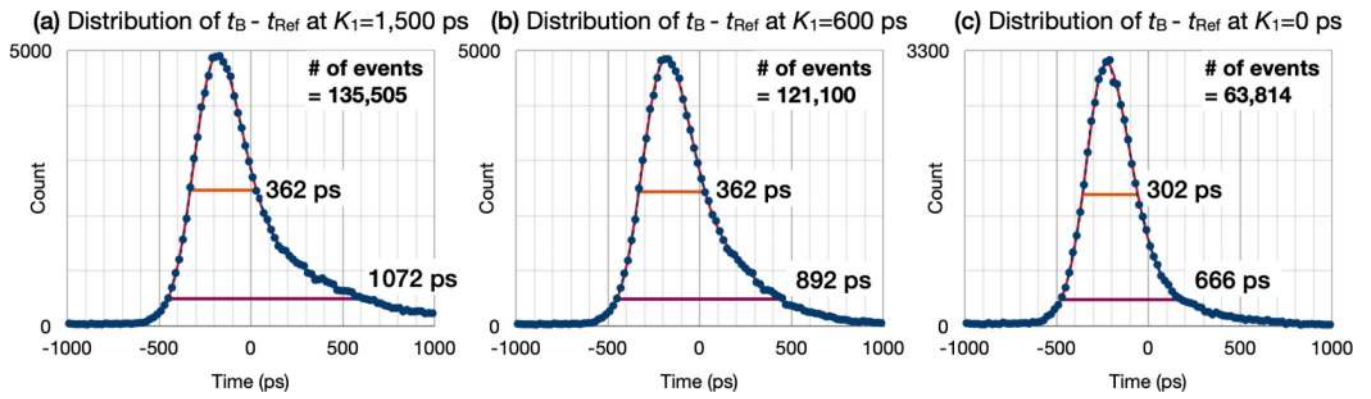Distributions of the trigger time differences between bottom and top SiPMs ($t_B - t_T$): experimental results (a) and simulation results (b).

(a) Distribution of $t_B - t_{Ref}$ at K_1=1,500 ps   **(b)** Distribution of $t_B - t_{Ref}$ at K_1=600 ps   **(c)** Distribution of $t_B - t_{Ref}$ at K_1=0 ps

Figure 4.

Coincidence timing spectra with different K_1 values of 1,500 ps (a), 600 ps (b), and 0 ps (c) when trigger times from the bottom SiPM were used.
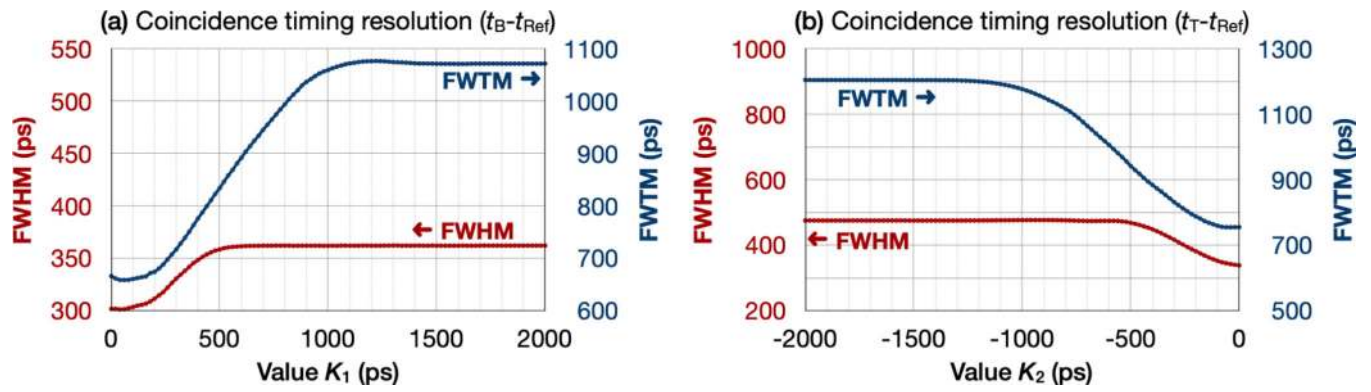
Figure 5.
FWHM and FWTM of each coincidence timing spectrum using experimental data as a function of K_1 and K_2 when trigger times from either the bottom (a) or top (b) SiPM were used.
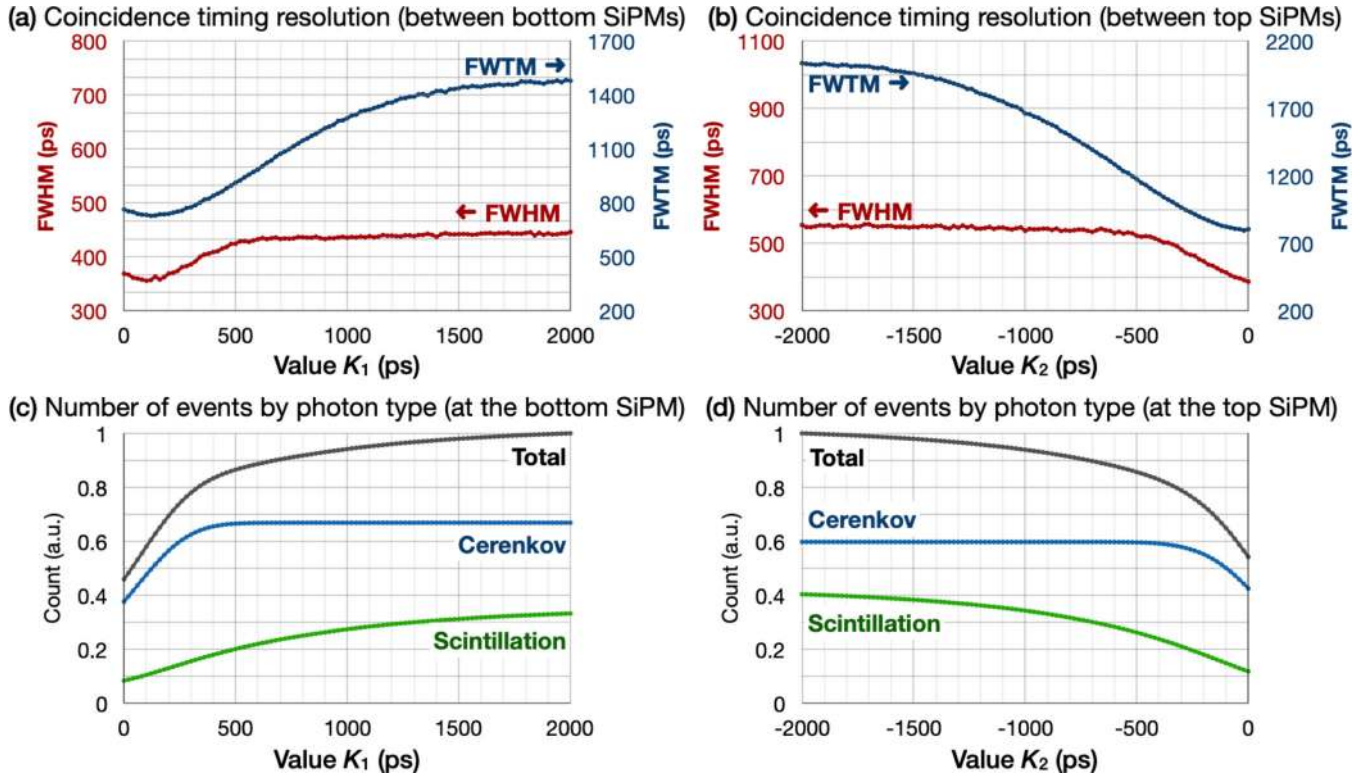
Figure 6.
FWHM, FWTM (a), (b), and counts (c), (d) using simulation data as a function of K_1 and K_2 when either the top (a), (c) or bottom (b), (d) SiPM used.
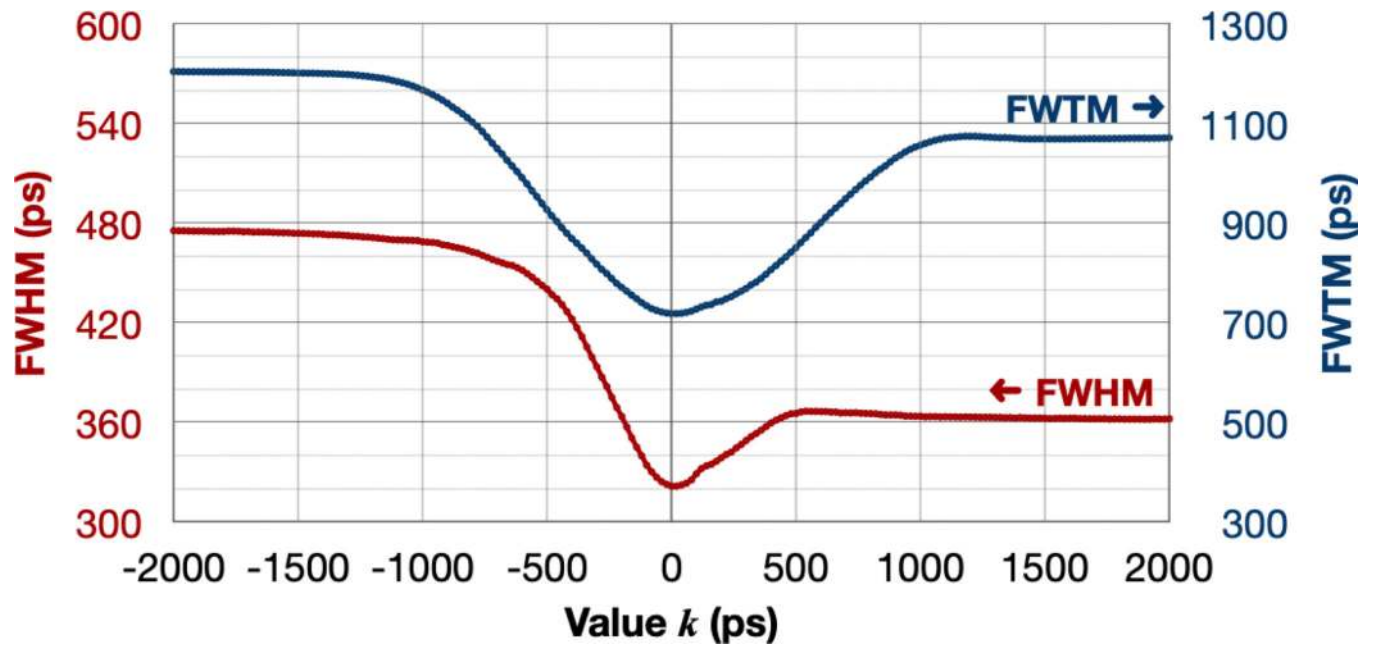
Figure 7.
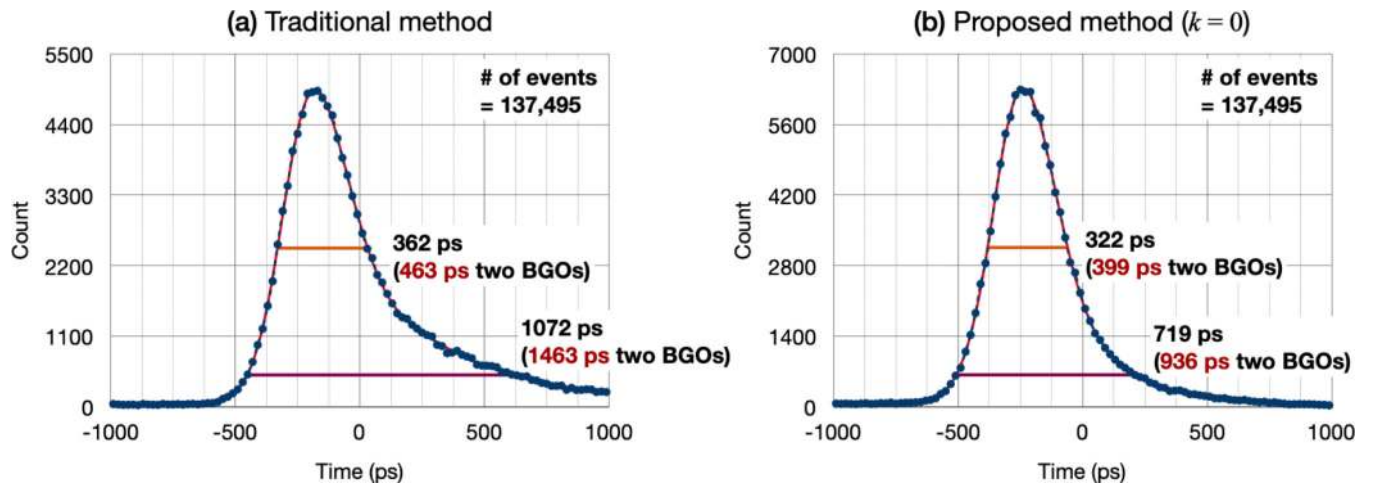FWHM and FWTM calculated using the proposed method as a function of *k*.

Figure 8.
FWHM and FWTM of coincidence timing spectra from experimental data using only trigger times from the bottom SiPM (a) and the proposed method (*k*=0) (b).
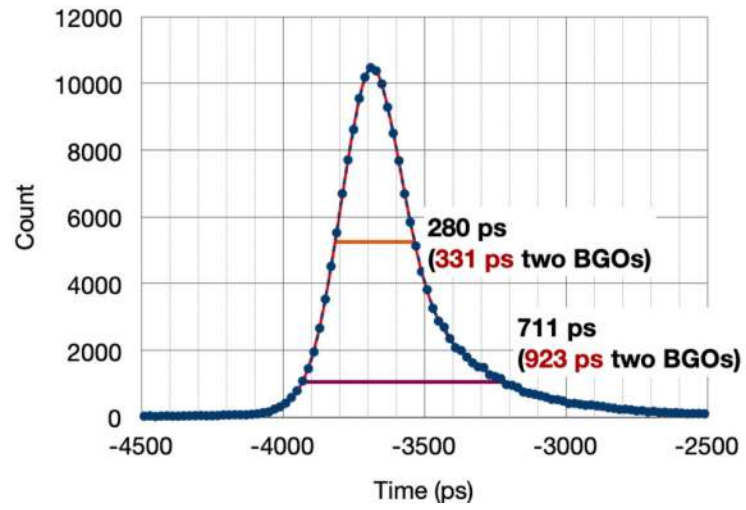
Proposed method ($k = 0$) and high-bandwidth amplifiers

Figure 9.
FWHM and FWTM of coincidence timing spectra from experimental data using the proposed method (k=0) and high-bandwidth amplifiers.

Table 1.

Estimated coincidence timing resolution according to the source of trigger time at the BGO detector

Source of trigger time		t_B	t_T	$\dfrac{t_B + t_T}{2}$	Proposed method (Equation 1, $k = 0$)
Coincidence timing	FWHM (ps)	463	636	522	399
resolution	FWTM (ps)	1,463	1,657	1,341	936